Simulating Observations of Southern Ocean Clouds and Implications for Climate

Andrew Gettelman[1], Charles Bardeen[1], Christina S. McCluskey[2], Emma Järvinen[3], Jeffrey Stith[1], and Chris Brethenton[4]

[1]National Center for Atmospheric Research (UCAR)
[2]National Center for Atmospheric Research
[3]Karlsruhe Institute of Technology
[4]University of Washington

November 24, 2022

Abstract

Southern Ocean (SO) clouds are critical for climate prediction. Yet, previous global climate models failed to accurately represent cloud phase distributions in this observation-sparse region. In this study, data from the Southern Ocean Clouds, Radiation, Aerosol, Transport Experimental Study (SOCRATES) experiment is compared to constrained simulations from a global climate model (the Community Atmosphere Model, CAM). Nudged versions of CAM are found to reproduce many of the features of detailed in-situ observations, such as cloud location, cloud phase and boundary layer structure. The simulation in the latest versions of the model has improved its representation of SO clouds with adjustments to the ice nucleation and cloud microphysics schemes that permit more supercooled liquid. Initial comparisons between modeled and observed hydrometeor size distributions suggest that the modeled hydrometeor size distributions are close to observed distributions, which is remarkable given the scale difference between model and observations. Comparison to satellite observations of cloud physics is difficult due to model assumptions that do not match retrieval assumptions. Some biases in the model's representation of SO clouds and aerosols remain, but the detailed cloud physical parameterization provides a basis for process level improvement and direct comparisons to observations. This is critical because cloud feedbacks and climate sensitivity are sensitive to the representation of Southern Ocean clouds.

Simulating Observations of Southern Ocean Clouds and Implications for Climate

A. Gettelman[1], C. G. Bardeen[1], C. S. McCluskey[1], E. Järvinen[1], J. Stith[1], C. Bretherton[2]

[1]National Center for Atmospheric Research, Boulder, CO, USA
[2]Department of Atmospheric Sciences, University of Washington, Seattle, WA , USA

Key Points:

- A nudged GCM can qualitatively reproduce detailed in-situ aircraft observations, including size distributions
- New model simulations have increased supercooled liquid clouds over the Southern Ocean
- Southern Ocean supercooled liquid clouds are important for climate prediction

Corresponding author: A. Gettelman, `andrew@ucar.edu`

Abstract

Southern Ocean (SO) clouds are critical for climate prediction. Yet, previous global climate models failed to accurately represent cloud phase distributions in this observation-sparse region. In this study, data from the Southern Ocean Clouds, Radiation, Aerosol, Transport Experimental Study (SOCRATES) experiment is compared to constrained simulations from a global climate model (the Community Atmosphere Model, CAM). Nudged versions of CAM are found to reproduce many of the features of detailed in-situ observations, such as cloud location, cloud phase and boundary layer structure. The simulation in the latest versions of the model has improved its representation of SO clouds with adjustments to the ice nucleation and cloud microphysics schemes that permit more supercooled liquid. Initial comparisons between modeled and observed hydrometeor size distributions suggest that the modeled hydrometeor size distributions are close to observed distributions, which is remarkable given the scale difference between model and observations. Comparison to satellite observations of cloud physics is difficult due to model assumptions that do not match retrieval assumptions. Some biases in the model's representation of SO clouds and aerosols remain, but the detailed cloud physical parameterization provides a basis for process level improvement and direct comparisons to observations. This is critical because cloud feedbacks and climate sensitivity are sensitive to the representation of Southern Ocean clouds.

Plain Language Summary

Clouds over the Southern Ocean are critical for climate prediction, and may influence the evolution of global temperatures. Thus these clouds are important to represent properly in models; however, recent studies have revealed models inadequately represent Southern Ocean cloud occurrence and phase, which drive large biases in radiation and subsequent climate sensitivity. Observations from research aircraft over the Southern Ocean south of Australia are compared to simulations with a global climate model which is 'nudged' to reproduce the day to day cloud systems which are sampled. Despite being a coarse horizontal and vertical resolution, the model is able to reproduce many details of cloud phase and water content during the flights. However, the model has some biases, and these observations have been used to improve the model to better represent cloud phase. These results point to specific observational constraints for improving model simulations.

1 Introduction

Southern Ocean (SO) clouds are critical for climate, regulating both local energy input and interacting with the deep ocean circulation (Trenberth & Fasullo, 2010). Earth System Models (ESMs) have been heavily biased in this region (Tsushima et al., 2006; Trenberth & Fasullo, 2010), with too much absorption of shortwave radiation, a result of too few clouds. Some models have mitigated the biases against observations with clouds that are too bright (Bodas-Salcedo et al., 2012; Lohmann & Neubauer, 2018). It has recently been realized that one major reason for these biases has been the incorrect phase of the clouds in models. SO clouds are mostly supercooled liquid water, while many climate models represent them as ice (e.g., Bodas-Salcedo et al., 2012).

The processes that maintain supercooled liquid clouds over the S. Ocean are complex, and not well constrained. Tan et al. (2016) found that SO low clouds were sensitive to the vapor deposition (Wegener-Bergeron-Findeisen, or WBF) process and ice nucleation. Vergara-Temprado et al. (2018) found SO cold-sector stratocumulous clouds were sensitive to ice nucleation schemes. McCluskey et al. (2018) found that the SO ice nucleating particle number concentrations were some of the lowest reported. Mace & Protat (2018) have found large discrepancies between satellite-derived and ship-based remote sensing cloud phase estimates; recent observations from O'Shea et al. (2017) suggest secondary ice production may be a contributing processes for ice formation in this

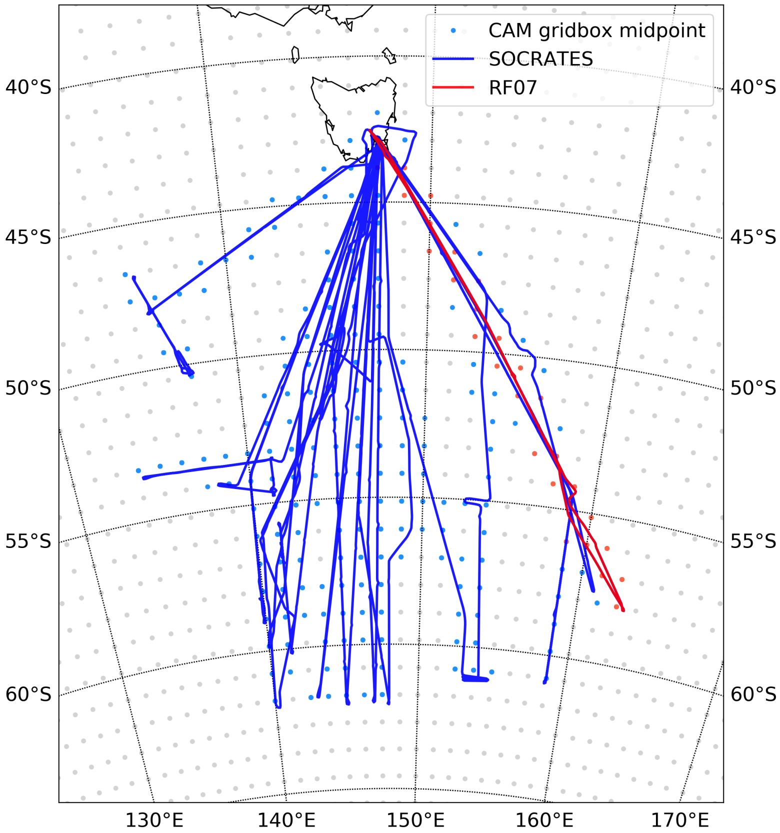

Figure 1. Map of SOCRATES mission flight tracks from the NSF G-V aircraft. Red is Flight RF07 on 31 January 2018 detailed later in the text. Solid dots indicate locations of CAM6 grid point centers used for comparison.

region and could contribute to explaining the discrepancies. SO supercooled liquid clouds have been identified as a significant contributor to cloud feedbacks and climate sensitivity: the response of the earth system to anthropogenic radiative forcing (Tan et al., 2016; Bodas-Salcedo et al., 2019; Gettelman et al., 2019).

To help better understand the processes controlling Southern Ocean Clouds, the Southern Ocean Clouds, Radiation, Aerosol, Transport Experimental Study (SOCRATES) was conducted January-March 2018 in the context of an international series of linked experiments in the Australian region of the S. Ocean. SOCRATES featured a heavily instrumented aircraft (the NSF G-V 'HIAPER' aircraft) with a payload of in-situ and remote sensing instrumentation (see Section 2.4).

Figure 1 illustrates the SOCRATES flight tracks from Hobart, Tasmania, Australia into the S. Ocean. Flights targeted different portions of extratropical cyclones as they tracked across the S. Ocean storm track South of Tasmania in January and February 2018.

As one of the key goals of SOCRATES was to evaluate and improve cloud and aerosol processes in ESMs, detailed simulations of the SOCRATES environment and flight tracks were conducted and compared to observations. In this work we describe constrained model simulations that enable even a coarse resolution climate model to be compared to detailed in-situ and remote sensing observations. We evaluate model simulations with a state of the art ESM, and conduct sensitivity tests of different cloud processes. We then illustrate how the observations can inform and constrain cloud processes which are critical for climate projections.

Section 2 contains a description of the model formulation, simulations and observations. Section 3 presents the core results and evaluation of the model simulations, including campaign averages, selected cases, sensitivity tests and the global implications. Discussion is in Section 4, and Conclusions and ideas for future work in Section 5.

2 Methods

2.1 Model

The Community Atmosphere Model version 6 (CAM6) is the atmospheric component of the Community Earth System Model version 2 (Danabasoglu et al., 2020). CAM6 features a two-moment stratiform cloud microphysics scheme, MG2, (Gettelman & Morrison, 2015; Gettelman et al., 2015) with prognostic liquid, ice, rain and snow hydrometeor classes. MG2 permits ice supersaturation, and links a physically based ice mixed phase phase dust ice nucleation scheme (Hoose et al., 2010) implemented in CAM6 with modifications for a distribution of contact angles by Wang et al. (2014), and accounting for preexisting ice in the cirrus ice nucleation of Liu & Penner (2005) as described by Shi et al. (2015).

MG2 is coupled to a unified moist turbulence scheme, Cloud Layers Unified by Binormals (CLUBB), developed by Golaz et al. (2002) and Larson et al. (2002) and implemented in CAM by Bogenschutz et al. (2013). CLUBB handles stratiform clouds, boundary layer moist turbulence and shallow convective motions. CAM6 also has an ensemble plume mass flux deep convection scheme described by Zhang & McFarlane (1995) and Neale et al. (2008), which has very simple microphysics. The radiation scheme is The Rapid Radiative Transfer Model for General Circulation Models (RRTMG) (Iacono et al., 2000).

CAM6 is the result of a long development process that concluded near the end SOCRATES observations described here. For comparison (see below) we also include simulations using the older version of the model, CAM5 (Neale et al., 2010). CAM5 had a different treatment of boundary layer and shallow convective turbulence (Bretherton & Park, 2009; Park & Bretherton, 2009) and a simpler treatment of cloud microphysics and supercooled liquid (Morrison & Gettelman, 2008; Gettelman et al., 2010) with ice nucelation in the mixed phase a function of temperature following Meyers et al. (1992).

2.2 Model Configuration

CAM6 is run in a 'nudged' (or Specified Dynamics) configuration with standard 32 vertical levels from the surface to 3hPa, a 30 minute timestep and horizontal resolution of 0.9° latitude by 1.25° longitude. The resolution of the model is shown by marking the model gridpoint centers on Figure 1. Nudging means that winds and optionally temperatures are relaxed to an analysis system, in this case the NASA Modern-Era Retrospective analysis for Research and Applications, version 2 (MERRA2) (Molod et al., 2015). Data is read in from files every 3 hours, and linearly interpolated to the model time. Sea Surface Temperatures (SSTs) are also read from the MERRA2 analysis. Two critical elements are worth noting. First, the model uses a 24 hour relaxation time to the MERRA2 winds and temperatures. Second, the MERRA2 analysis is interpolated in the vertical to the CAM6 vertical level structure. These two adjustments were found to enable a global simulation to reproduce the top of atmosphere balance of a free running CAM6 simulation to within 2 Wm^{-2}, so that the 'climate' of the free running simulation is the same.

Simulations were spun up for 1 year using 2017 meteorology. The model was then restarted from January 1, 2018, and run over the SOCRATES flight period for 2 months. Model output is archived along the flight tracks and is sampled at 1 minute resolution.

2.3 Sensitivity Tests

We conduct several sensitivity tests with the same configuration described above (Table 1). *CAM6* is the control case. *CAM5* uses physical parameterizations as described by Neale et al. (2010). *Meyers* switches the CAM6 dust dependent mixed phase ice nucleation (Hoose et al., 2010; Wang et al., 2014) back to the temperature dependence of Meyers et al. (1992). *Berg0.25* reduces the efficiency of the vapor deposition (Wegner-Bergeron-Findeisen, or WBF) process by 75%. *SIP* experiments modify the Secondary Ice Production in the MG2 scheme Cotton et al. (1986) by either setting it to zero (*SIP0*) or increasing it by a factor of 5 (*SIP5*).

We also perform several different experiments in response to the initial comparisons in Section 3. These focus around first altering the representation of rain formation (autoconversion). First we modify the existing formation by reducing autoconversion by a factor of 10 (*Auto/10*) or by replacing the modified formulation of Khairoutdinov & Kogan (2000) with that of Seifert & Beheng (2001), as discussed by Gettelman (2015) (*SB2001*). Second, the *Eta* experiment reduces the dispersion of the size distribution of cloud drops (η in Morrison & Gettelman (2008)) by switching from the formulation of Rotstayn & Liu (2003) used in CAM6 back to that of Martin et al. (1994) used in CAM5 (Morrison & Gettelman, 2008). Two additional simulations are discussed: increasing IN for mixed phase clouds with temperatures above -10°C in CAM6 (*In10-10*) and narrowing the CAM6 rain size distribution by setting the shape parameter of the gamma distribution (μ) to a non-zero value (*MuR=5*).

We also explore the impact of nudging, by running additional simulations with temperatures and winds fixed to MERRA2 (*Fix T*), only U and V nudging and free running temperatures (*Free T*) and using a relaxation time scale of 1 hour nudging for winds and temperatures (*Nudge 1hr*). These experiments help elucidate whether any temperature biases are from CAM or from the input (MERRA2) analysis. Verification of temperatures will be against SOCRATES in-situ data from the aircraft and dropsondes.

2.4 SOCRATES Data

During SOCRATES the U.S. National Science Foundation (NSF) HIAPER aircraft was equipped with a suite of in-situ and remote sensing instruments. In-situ instruments included cloud microphysical probes for measurement of both liquid and ice phase. Cloud droplet spectra was measured with the Cloud Droplet Probe (CDP; Lance et al. (2010)) that provides cloud droplet PSDs for particle diameters (D_p) of $2 < D_p < 50$ micron. The CDP Particle Size Distributions (PSDs) can be integrated to get an estimate of the liquid water content (LWC). Another measure of the LWC was delivered by the King probe (King et al., 1978).

A 2D stereo probe (2DS) was used to determine PSDs and mass concentrations from particle shadow-graphs for particles in the size range of $0.05 < D_p < 3.2$ mm. The size limit of 2DS is 0.01 mm but here particles below 0.05 mm are not considered due to uncertainties in the probe's depth of field and sample area. 2DS has a set of four arms that deliver shadow-graphs both in the horizontal (H) and vertical (V) direction. During SOCRATES

Table 1. Sensitivity Tests with nudged CAM simulations

Name	Description
CAM6	Control
CAM5	CAM5 Physical Parameterizations
Meyers	Meyers et al. (1992) Mixed Phase Ice Nuc
Berg0.25	WBF efficiency $1 \rightarrow 0.25$
SIP0	No Secondary Ice Production
SIP5	5 x Secondary Ice production
Auto/10	Autoconversion / 10.
SB2001	Seifert & Beheng (2001) autoconversion formulation
Eta	Reduced width of size distribution
In10-10	CAM6 with increased ice nucleation (rate)
MuR=5	Non-zero rain shape parameter ($\mu = 5$)
Fix T	MERRA U, V, and T
Free T	No T nudging (U, V only)
Nudge 1hr	Nudging reduced from 24hr to 1hr

the vertical direction was not working properly and, therefore, only horizontal data (2DS-H) was used.

Remote sensing probes included Radar, Lidar and Dropsondes. The HIAPER Cloud Radar (HCR) and a Hyper Spectral Lidar (HSRL) (EOL, 2018) were also used on the aircraft. The orientation of the radar and lidar was changed during the flight to point up or down as appropriate. A description of the dropsonde data, including data processing and quality assurance methods are provided in Young (2018) and Young & Vömel (2018).

Additional information on HIAPER airborne data (e.g. temperature, humidity, winds, pressure, position) and data processing methods is provided by EOL (2018) and at https://www.eol.ucar.edu/aircraft-instrumentation.

2.5 Research Flight 7

In order to present the results and show impacts, we will show campaign averages of all flights, but will also focus on a particular sample flight that is representative of many flights from SOCRATES. We focus on Research Flight 7 (RF07), which took place on 31 January 2018. This flight (the red line in Figure 1) targeted a region of clouds in the cold sector of an extratropical cyclone South of Macquarie island (54.6° S, 158.9° E). The clouds were of a type that kept 'disappearing' in forecast models into a broken cloud deck, while satellite images continued to show solid cloud cover. The models being used in which such clouds disappeared included the European Centre for Medium Range Weather Forecasts (ECMWF) Integrated Forecast System (IFS), the National Oceanic and Atmospheric Administration (NOAA) Global Forecast System (GFS) and the Australian Community Climate and Earth-System Simulator (ACCESS).The composite radar image from RF07 is illustrated in Figure 2.

As illustrated in Figure 2, RF07 featured broken cumulus cloud between Hobart and Macquarie Island at 56°S. This is also seen in a Himawari-8 visible satellite image from 0600 UTC (Figure 3). After Macquarie island at about 330 UTC the aircraft descended to above the boundary layer and began cloud sampling with an above cloud leg over a supercooled air mass. Cloud top was about 1.5km for the whole layer, and the surface was cloud free. The cloud deck was solid on top, but thin with cellular structure.

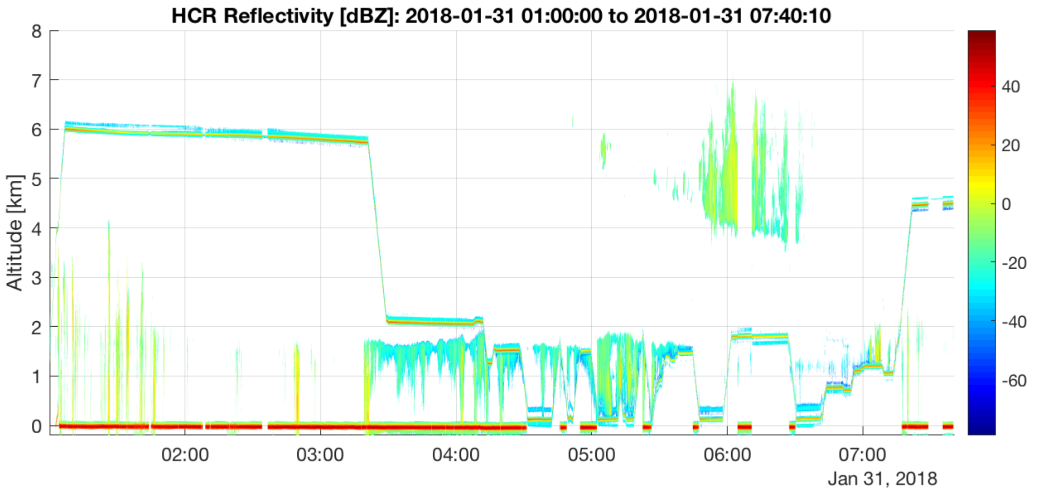

Figure 2. HIAPER Cloud Radar data from SOCRATES Research Flight 7 (RF07) illustrating flight altitude (thin red line) and observed clouds over time. The color bar indicates reflectivity in dBz.

Figure 4 is a visible wing camera image of the cloud layer at 410z just before turning north (58°S), illustrating it was optically thick. There were spots where the ocean was visible through small holes in the cloud. There was some thin cloud at 4.5-6km in this region, seen in the distance of the image in Figure 4.

The plane then headed north, sampling in and out of the cloud layer. There was pretty significant probe icing in the cloud, and the temperatures were just below freezing (see Temperature curtain in Figure 5). Near Macquarie island (500 UTC on the return) there were multiple cloud layers, with more extensive cloud and drizzle. Mixed phase graupel or snow was visible in some shafts from the plane and on the particle instruments. North of Macquarie island the lower cloud deck was more broken, and a shallow cumulus deck extended from about 1-2km.

3 Results

In order to better characterize the flights, we show examples of model and observational comparisons from RF07, then show how this generalizes to averages over the whole campaign and the model climatology. We use observations from the aircraft as well as broader scale satellite observations.

3.1 RF07 Results

Figure 5 illustrates temperatures along the flight track from RF07 and the base *CAM6* nudged simulation. Model temperatures are generally within 1-2° of the aircraft at all times, as the temperatures are nudged to MERRA2 with a 24 hour relaxation time. The top of the boundary layer in the cloud layer from 4 to 6 UTC is just below the freezing level, with the ocean surface just above freezing.

The structure of the temperature biases is more easily seen in a comparison to the last dropsonde at 3:44 UTC (Figure 6). At 800-750 hPa, right at the top of the boundary layer, *CAM6* is missing the temperature inversion seen in the observations. The inversion is much finer vertical resolution than the model, but even the binned average has a bias of several °C in this layer. The lack of resolution of the inversion results in high

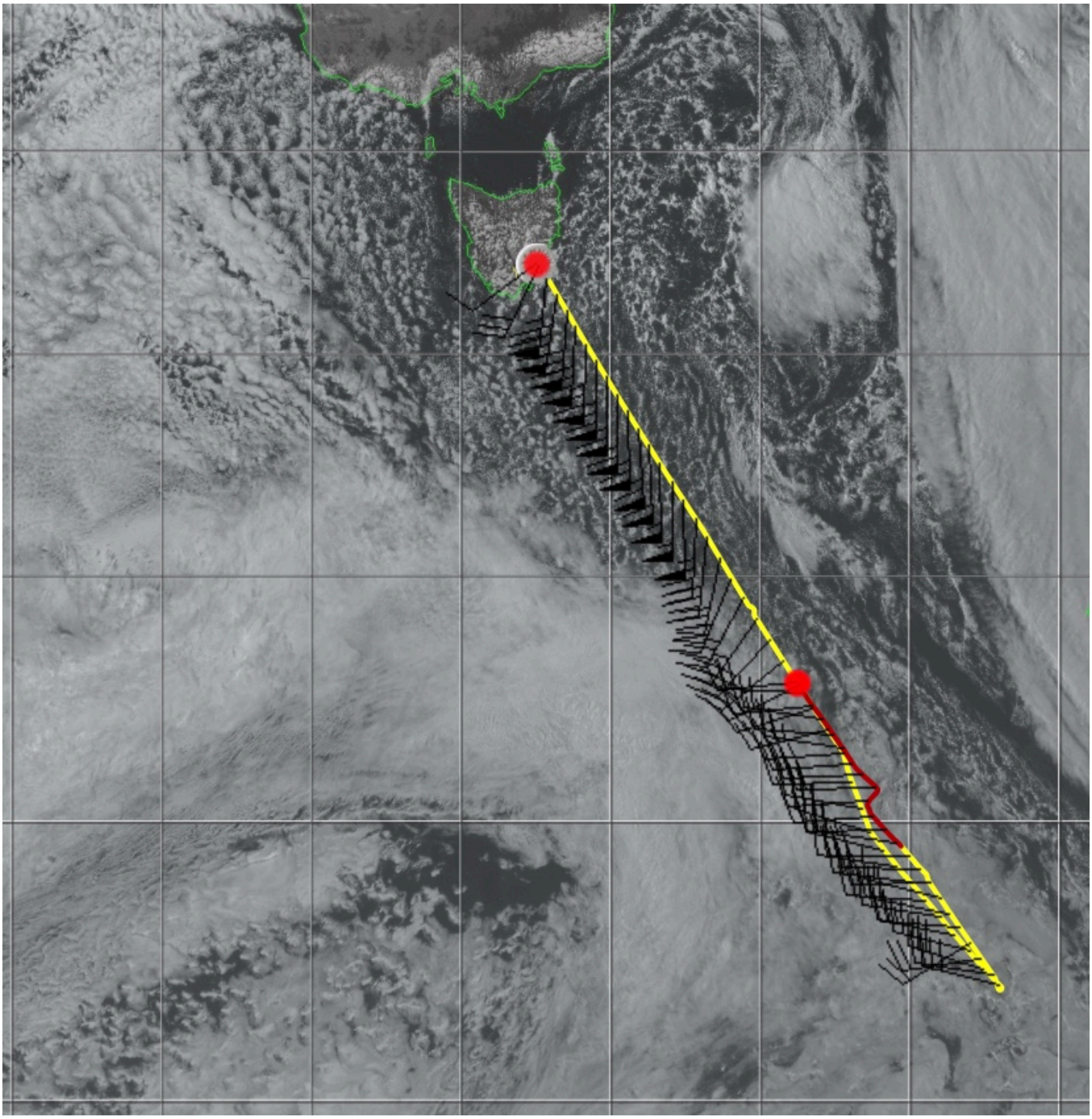

Figure 3. Himawari-8 Visible satellite image at 600 UTC, 31 January 2018 showing cloud field. Also indicated is the aircraft flight track up to 600 UTC with wind vectors from aircraft observations along the flight track. Yellow indicates the flight track, red 500–600 UTC.

Figure 4. Aircraft forward camera image from 410 UTC near turnaround latitude.

humidity in the layer above the boundary layer top. There is a moderate humidity bias in the boundary layer up to 800 hPa in *CAM6*. While the zonal wind is well reproduced (perhaps too high right near the surface), the meridional wind has a significant bias.

To check whether this bias is the result of the nudging data, we fixed the temperatures and winds to MERRA2 analysis and re-ran the simulation (*Fix T*). Figure 7 shows the comparison between MERRA2 winds and temperatures and the dropsonde observations. The temperature bias is significantly reduced, leading to improved humidity above the boundary layer. But the wind biases remain. The zonal wind bias is larger than the base case at the top of the boundary layer. Thus the wind biases may come from the input reanalysis data, while the temperature bias and inversion bias seem to be a result of CAM simulations pushing the model away from the analysis. Experiments with 1 hour nudging (*Nudge 1hr*), or no temperature nudging (*Free T*), confirm this trend: 1 hour nudging has an intermediate temperature bias between analysis temperatures (Figure 7) and 24 hour nudged temperatures (Figure 6), while no temperature nudging yields a larger bias than 24 hour nudging in Figure 6.

Figure 8 illustrates that these temperature biases are a general feature of the CAM6 simulations for the whole campaign (119 dropsondes). There are consistent $\sim 1^{\circ}$ (range of -2.5 to 0) temperature biases at the top of the PBL, indicating the lack of an inversion in the base CAM6 24 hour nudged simulation. Associated with this temperature bias is a positive $\sim 20\%$ relative humidity bias, nearly half of which is due to the colder temperatures. Figure 8B indicates that this is not due to the input data, as the MERRA2 reanalysis temperatures are on average only 0.2 °C colder than the dropsondes (range of -1 to 0). This also significantly reduces the humidity bias (Figure 8D), and reduces the error due to temperature (compare to red line in Figure 8C and D). Note that the

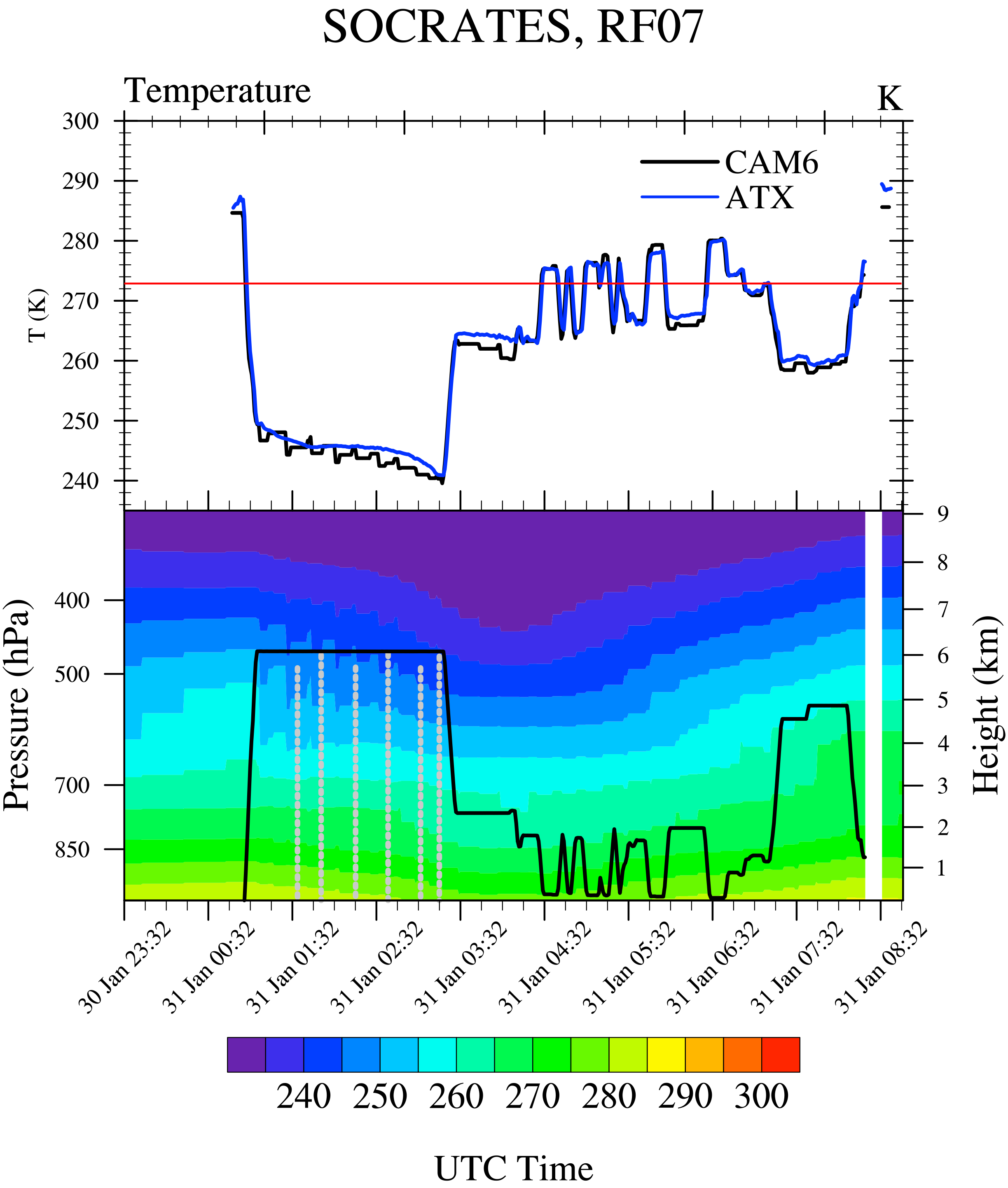

Figure 5. Temperatures along the flight track from RF07, showing the entire flight as a function of time from right to left. Note that latitude decreases (southward flight to 4:11 UTC and then increases again as the plane turned around. Freezing level (273K) is the thin red line. The bottom panel shows aircraft altitude (solid black) and dropsonde locations (dashed gray) on top of the simulated temperature curtain from the CAM6 base case. Top panel illustrates the aircraft temperature at flight level (ATX black) and model temperature (CAM6) interpolated to the flight level.

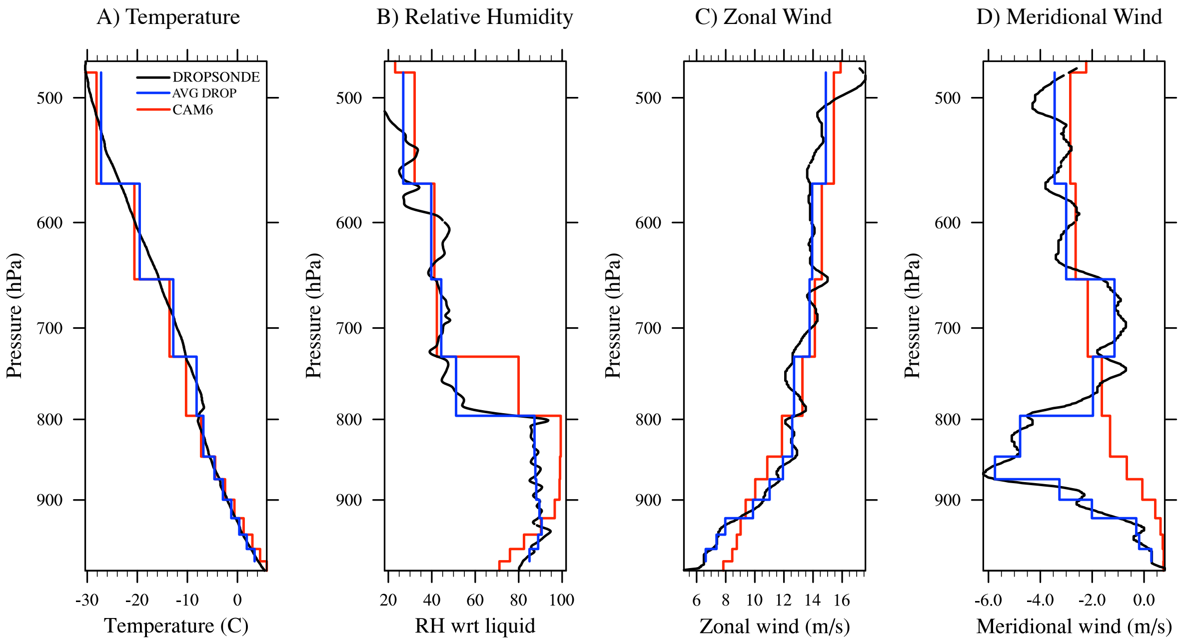

Figure 6. Comparison of dropsonde between CAM6 (red), dropsonde (black), and dropsonde binned to CAM6 levels (blue). (A) Temperature (B) Relative Humidity with respect to Liquid (RH wrt liquid, %), (C) Zonal Wind (m/s) and (D) Meridional Wind (m/s).

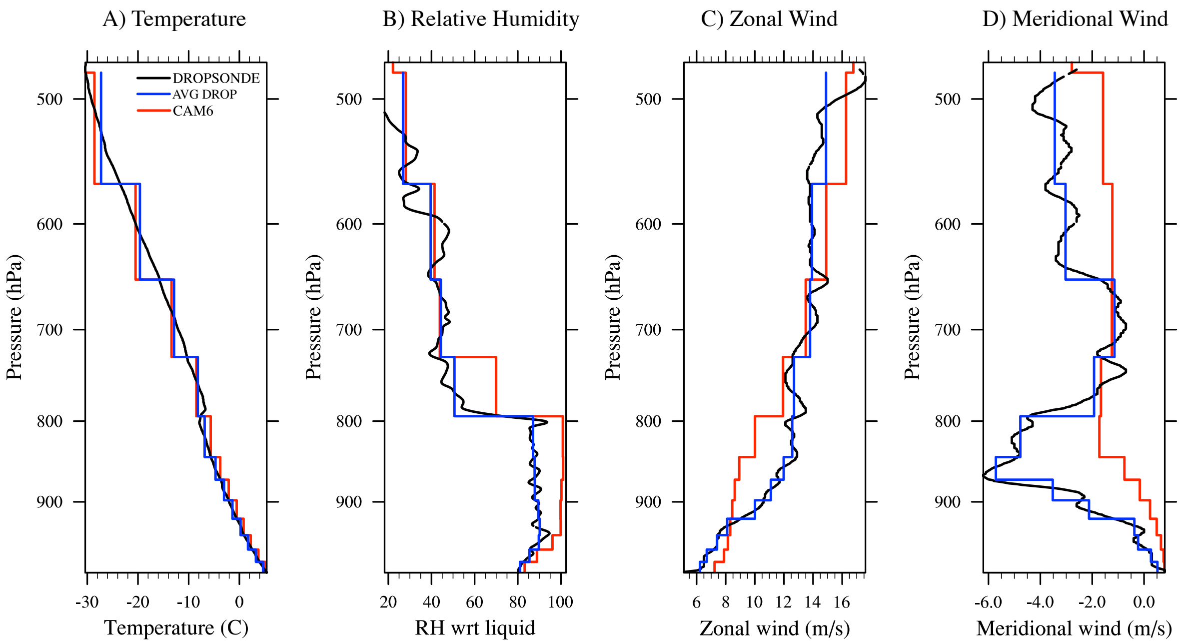

Figure 7. As for Figure 6 but for a CAM6 simulation with fixed MERRA-2 temperatures and winds.

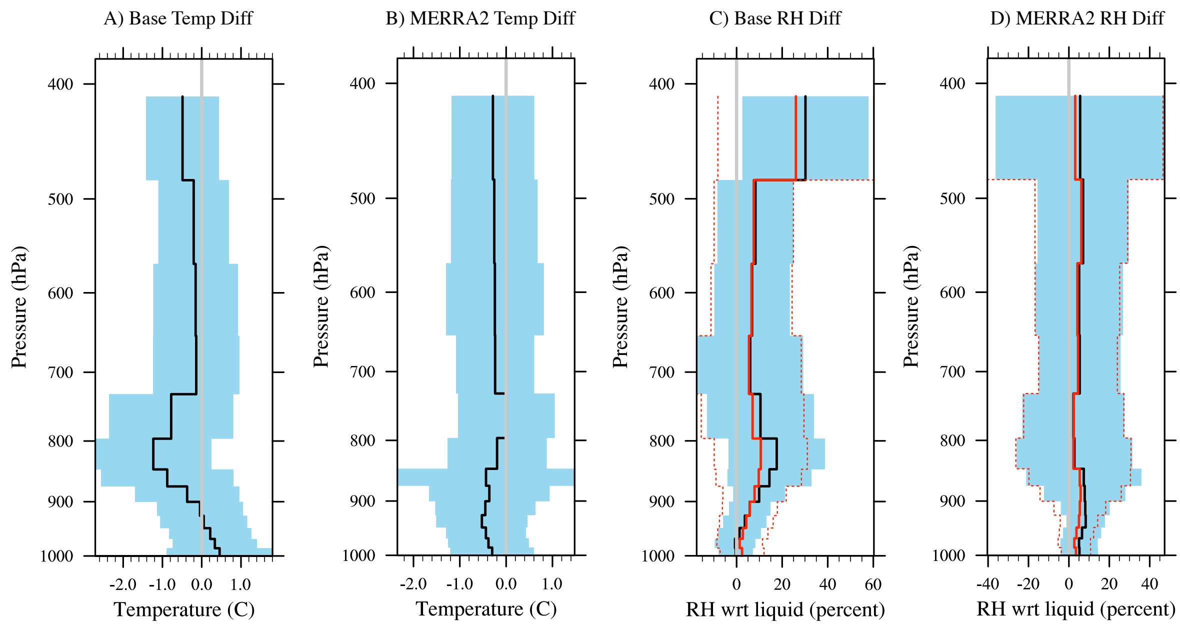

Figure 8. Average temperature (A and B) and relative humidity (C and D) differences from SOCRATES dropsondes at the sonde locations and times from CAM6 24 hour nudged simulation (A and C) and using fixed MERRA-2 Temperatures (B and D). Red line in C and D (RH plots) is the RH estimated assuming the radiosonde temperature for saturation (no temperature error). Light blue shading is the range of all radiosonde differences, red dashed lines in C and D are the range of all RH differences where simulated RH is estimated using model specific humidity and saturation humidity is estimated using dropsonde temperature.

fixed temperature (MERRA2) simulation does have interactive (not fixed) specific humidity.

Figure 9 illustrates a curtain of cloud hydrometeors (liquid, ice and supercooled liquid) observed and simulated for RF07. The CDP and F2DS were used to estimate liquid and ice mass concentrations, respectively. CAM6 simulates a boundary layer cloud deck throughout the whole flight, with some higher ice clouds on the return near Hobart (from 5 to 7 UTC). The cloud layer sampled in the observations and model from 4-6 UTC is a mix of supercooled liquid and ice, of about the same mass concentration. Clouds are present at the top of the PBL, with no cloud in the surface layers. The dominant hydrometeor for much of this time in both models and observations is supercooled liquid, which appears to be about the right mass over the flight, with wide variation of the liquid and ice in the model and observations.

SOCRATES is a unique campaign for its extensive sampling of cloud drop and crystal size distributions in Southern Ocean supercooled liquid clouds. CAM6 is uniquely placed to take advantage of this evaluation opportunity, since the two moment microphysics scheme (Morrison & Gettelman, 2008; Gettelman & Morrison, 2015) has a prognostic representation of the size distribution. Here we use the moments of the size distribution with the functional form of the gamma distribution assumed in the MG2 scheme, to reconstruct the size distribution for all the hydrometeors (liquid, ice, rain and snow) in CAM6, and compare this to observations from the suite of instruments on the GV aircraft during SOCRATES. Figure 10 illustrates the reconstructed distributions for (A) All, (B) Cold (T$<$ 0°C) and (C) Warm (T$>$ 0°C) clouds at pressures greater than 750hPa,

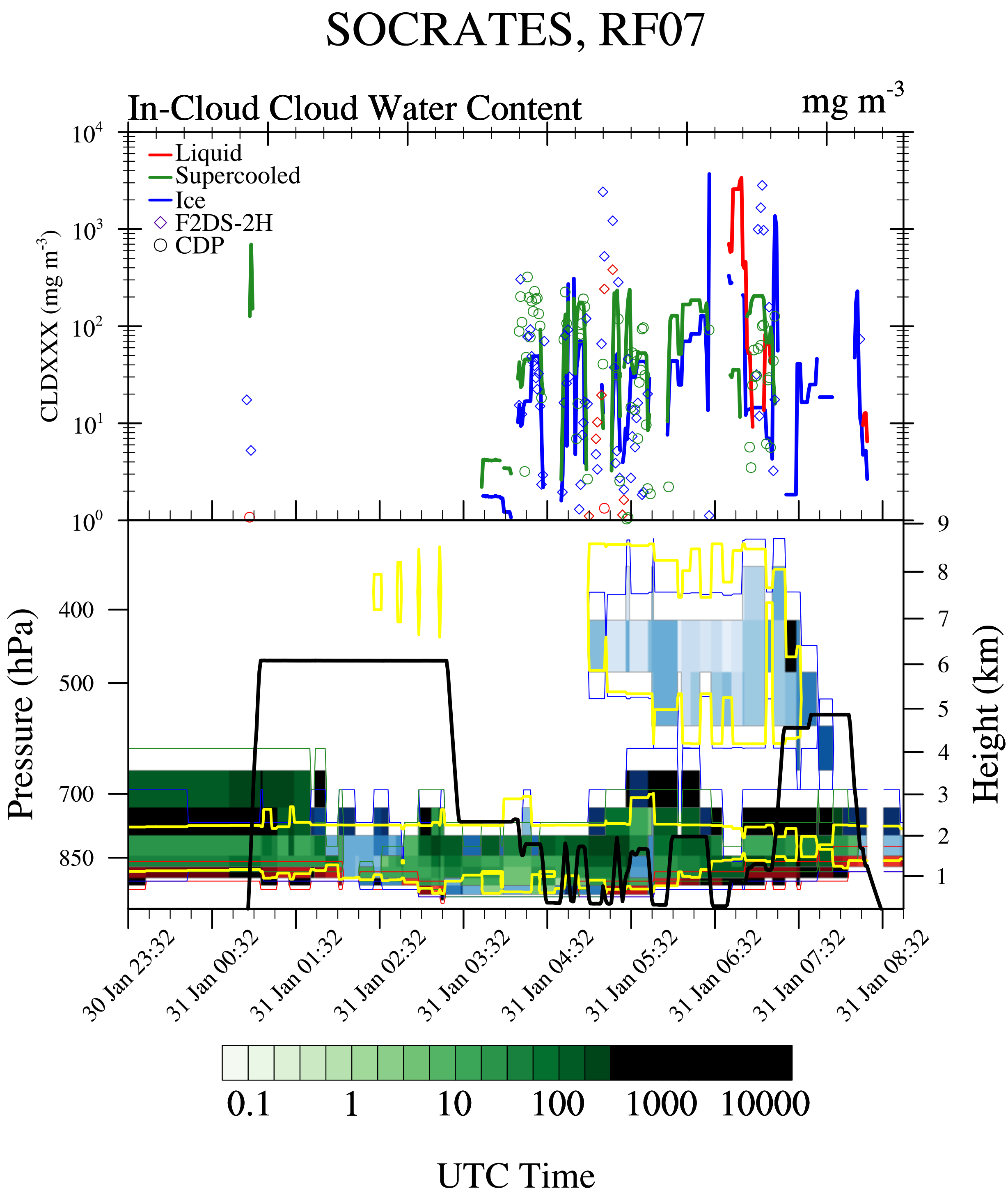

Figure 9. Cloud hydrometeors along the flight track from RF07, showing the entire flight as a function of time from right to left. Note that latitude decreases (southward flight to 4:11 UTC and then increases again as the plane turned around. The bottom panel shows aircraft altitude (solid black) on top of the simulated cloud mass from the CAM6 base case. Top panel illustrates the aircraft liquid (red), ice (blue) and supercooled liquid (green) at flight level and model (CAM6) liquid (red), ice (blue) and supercooled liquid (green) interpolated to the flight level. Bottom panel shows the dominant (largest mass) hydrometeor by color from the simulation (Liquid = Red, Ice = Blue and Supercooled liquid = Green). Increased intensity of the color indicates higher water content. The colorbar shows the scale for supercooled liquid. Yellow contour is cloud fraction greater than 10%. The model was sampled every minute, and the observational data were also average to one minute.

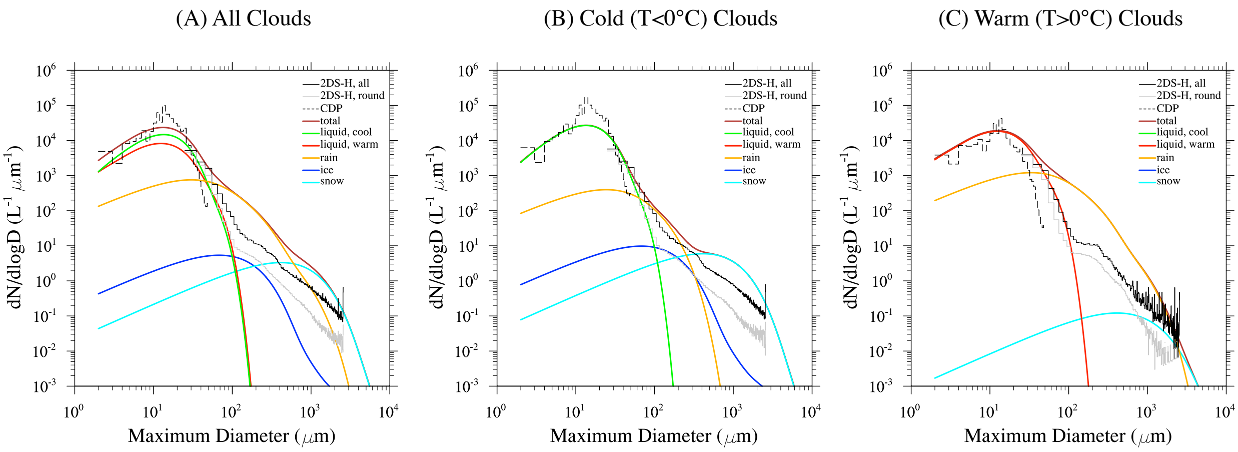

Figure 10. Size distributions from observations (thin lines) and reconstructed model hydrometeor size distributions (thick colored lines) for low level clouds (P>750mb) as indicated in the legend. Selected cloud probe data shown as 2DS for all particles (thin black) and round particles (thin gray) and CDP (thin black dotted). (A) All clouds, (B) Cold clouds, (C) Warm clouds. Model is sampled along the flight track at aircraft altitude.

to isolate shallow clouds near the surface. The model is sampled along the flight track at aircraft altitude.

Note the extreme scale separation for this comparison. Observed size distributions for in-situ instruments are constructed from 1 hertz data, representing a sample volume of few cm^2 cross section and 150m of flight distance (in 1 second), with about 5000 samples total. Simulated size distributions are assumed functional averages of a single 'in-cloud' quantity per grid volume, typically 100km x 100km horizontal by 200m vertical. Given the limitations of a functional size distribution (e.g., fixed width), CAM6 does a remarkably good job at reproducing size distributions observed from the aircraft. Individual flights have similar characteristics.

Several aspects are notable. First, the size distribution for warm liquid clouds looks reasonable (Figure 10C) with a peak between 10-20 μm. However, for cold clouds, in general there does not seem to be enough supercooled liquid (see below for a discussion of sensitivity tests), but this varies on a flight by flight basis and depends on the type of cloud. The size distribution appears to be broader than observed from the aircraft cloud probes, with not enough peak number concentration. The snow size distribution seems well reproduced (Figure 10B), but there appears to be too much warm rain (Figure 10C), leading to too many cloud drops between 100 and 1000 μm, though this is a difficult area for instruments to observe, and there are discrepancies between the instrumentation. A similar plot for only flight RF07 indicates slightly less warm rain, and slightly more liquid in the shallow clouds for this flight, but the amount of liquid is still under-represented relative to the measurements.

We conducted an experiment to reduce the width of the size distribution for liquid (*Eta*). This did indeed reduce the width to look more like the observations in Figure 10. However, decreased width does not significantly increase the number of supercooled liquid drops. There are small increases in the total liquid number seen with increases in liquid water associated with reduction of the autoconversion rate and increase in water (*Auto/10*), and decreases in total number and liquid water associated with the *SB2001* autoconversion experiment.

Narrowing the size distribution for rain from an exponential (shape parameter $\mu = 0$) to $\mu = 5$ (*MuR=5*), reduced the larger rain sizes as expected, but significantly increased rain mass, not improving the comparison to observations.

3.2 Sensitivity Tests

We now turn to sensitivity tests where we vary the model formulation to test how it impacts the cloud and radiation simulation in the SOCRATES region and how it compares to observations. For a broader perspective, we look at regional averages from satellite data for January and February 2018. These are taken from the Clouds and the Earth's Radiant Energy System (CERES) retrievals (Wielicki et al., 1996; Loeb et al., 2018). Specifically we use version 4.1 of the Energy Balance Adjusted Flux (EBAF) product (DOI: 10.5067/TERRA-AQUA/CERES/EBAF-TOA_L3B004.1) and of the Synthesis product (SYN) version 4.1 (DOI: 10.5067/Terra+Aqua/CERES/SYN1degMonth_L3.004A). We look at monthly averages for January and February 2018, as well as daily averages over this period, and long term 15 year climatologies to try to understand the model solutions and comparisons in a broader context (see Section 3.3 below).

Figure 11 illustrates regional (45-65°S, 135-160 °E) 2 month means from the simulations and CERES data for large scale quantities that are important for cloud physics and for driving radiative fluxes. Higher water amounts (LWP, Figure 11A) are found with *Fixed T* or 1 hour nudging (*Nudge 1hr*), and lower LWP with free running temps (*Free t*) or for the *CAM5* simulations. The revised Seifert & Beheng (2001) autoconversion scheme (*SB2001*) results in lower LWP, similar to *CAM5*. Ice Water Path (Figure 11B) is higher for *CAM5* and for reduced Bergeron (*Berg0.25*, vapor deposition) and the Meyers et al. (1992) empirical ice nucleation as a function of temperature (*Meyers*). Both *Berg0.25* and *Meyers* are elements of CAM5 physics. Less liquid and more ice is expected from these changes to phase partitioning.

The CERES SYN LWP product mean for these two months in the SOCRATES region is lower than most CAM simulations except the *CAM5* and *SB2001* simulations, though it is not that well correlated with CAM simulations on a day-to-day basis. Note that this is a different result than implied by the SOCRATES in-situ data in Figure 9, which will be analyzed further below. CERES LWP and IWP are estimated from an assumed particle size (10μm for liquid and 30 μm for ice) and a retrieved optical depth from infrared reflectance (CERES SYN Edition 4 Data Quality Summary). As such, particularly for ice water path, CERES may not match the observed SOCRATES ice and snow sizes (Figure 10). Accordingly we do not show the CERES IWP (0.2 kg m^{-2}), which is much larger than LWP in this region. In addition, CERES and modeled LWP includes the entire atmospheric column, whereas Figure 10 includes only pressures $>$ 750hPa, thus a subset of clouds. Even the 10μm liquid radius is significantly smaller than simulated (Figure 11D).

Thus the observational comparisons with CERES in Figure 11 with the exception of Short Wave Cloud Radiative Effect (SWCRE, Figure 11F) and cloud fraction (Figure 11C) are heavily derived products from CERES and are subject to large retrieval uncertainties, and likely provide a limited prospective (e.g., Mace & Protat, 2018).

Figure 11C indicates less total cloudiness for *CAM5* than the other simulations. CERES EBAF 4.1 total cloud amounts for the same region and a 2 month average of January and February 2018 are shown on the figure, and fall between *CAM5* and *CAM6* simulations. Total cloud area on a day to day basis is fairly well correlated between the CAM simulations (coefficient of 0.3 to 0.4). *CAM5* is slightly better correlated than *CAM6*. Cloud fraction is low in *CAM5*, while *CAM6* has too many, but the differences are small: ±5% around 89% cloud cover.

CAM5 simulated cloud top drop size (Figure 11D) is notably smaller than *CAM6* and its variants, and corresponding to larger cloud drop number (Figure 11E). The result of the smaller sizes, with less liquid and more ice, is reduced (less negative) cloud forcing over this 2 month period (Figure 11F). The CAM5 (Meyers et al., 1992) ice nucleation parameterization (*Meyers*) seems to be responsible for this, as it has results closer to *CAM5*. We also explored increasing ice nuclei for temperatures T>-10°C (*In10-10*), and this increased IWP to even larger values than CAM5 (off scale on Figure 11B). CAM5 has the often seen model bias of too few and too bright SO clouds.

Interestingly, the less negative SW cloud forcing (radiative effect) is associated with lower cloud optical thickness, with CERES having a lower mean optical thickness than most of the CAM simulations. Note that CERES optical thickness is derived from infrared radiances on geostationary satellites and MODIS, and also has assumptions in it. The *SB2001* simulation, with lower LWP and cloud optical depth, but higher cloud fraction and larger effective radius, as well as less ice water path (and significant supercooled liquid), seems to best reproduce the CERES observations during the SOCRATES period. The SW Cloud Radiative Effect (Figure 11) is similar to CERES with similar optical thickness but too much cloud cover.

With respect to some of the other sensitivity tests, it is notable that adjusting the Secondary Ice Production (SIP) parameterization does not do much to the water path or number concentration, whether it is turned off (*SIP0*) or increased (*SIP5*). As noted, *Meyers* makes ice and liquid partitioning (and radiative effects) look more like *CAM5*, and is a big reason for the difference between model versions over the S. Ocean. These results demonstrate that the radiative properties of SO clouds in CAM, are sensitive to the ice nucleation scheme, similar to findings by Tan et al. (2016). This is discussed further in Section 3.3 below. Changing autoconversion (*SB2001* and *Auto/10*) has large impacts on LWP and cloud radiative properties.

Nudging has a non-negligible impact on water and ice partitioning. *FixT* and *Nudge 1hr* have less T bias, but higher cloud water (Figure 11A) and stronger cloud forcing (Figure 11G). The free running temperature simulation (*Free T*) has less cloudiness (Figure 11C), smaller sizes (Figure 11D) and reduced magnitude of SW Cloud Radiative Effect (Figure 11F). But the PBL structure has a larger bias in *Free T* (Figure 8).

As a more detailed illustration and comparison to SOCRATES observations, Figure 12 illustrates a simulation of flight RF07 with *CAM5* cloud microphysics, for comparison to Figure 9. *CAM5* features the Meyers et al. (1992) representation of ice nucleation as a function of temperature, and diagnostic precipitation, and so there is very little supercooled liquid water. This does not match observations in the top panel of Figure 12, where the *CAM5* simulation has ice (blue) and some warm liquid (red), but almost none of the supercooled liquid water (green) seen in the observations. This is clear indication that the revisions to cloud phase representation and partitioning in *CAM6* are an improvement over *CAM5* when compared to SOCRATES observations, even if the overall radiative effects in *CAM5* are closer to CERES (Figure 11F). The *SB2001* simulation has improved SW CRE (Figure 11F), but maintains supercooled liquid similar to CAM6 in Figure 9.

One additional note is that in CAM5 clouds are present all the way down to the lowest model layer ('stratofogulus'), which was not observed during RF07 or other flights. This improvement is likely related to the new unified moist turbulence scheme (CLUBB), in which turbulence is driving cloud formation, in better agreement with observations.

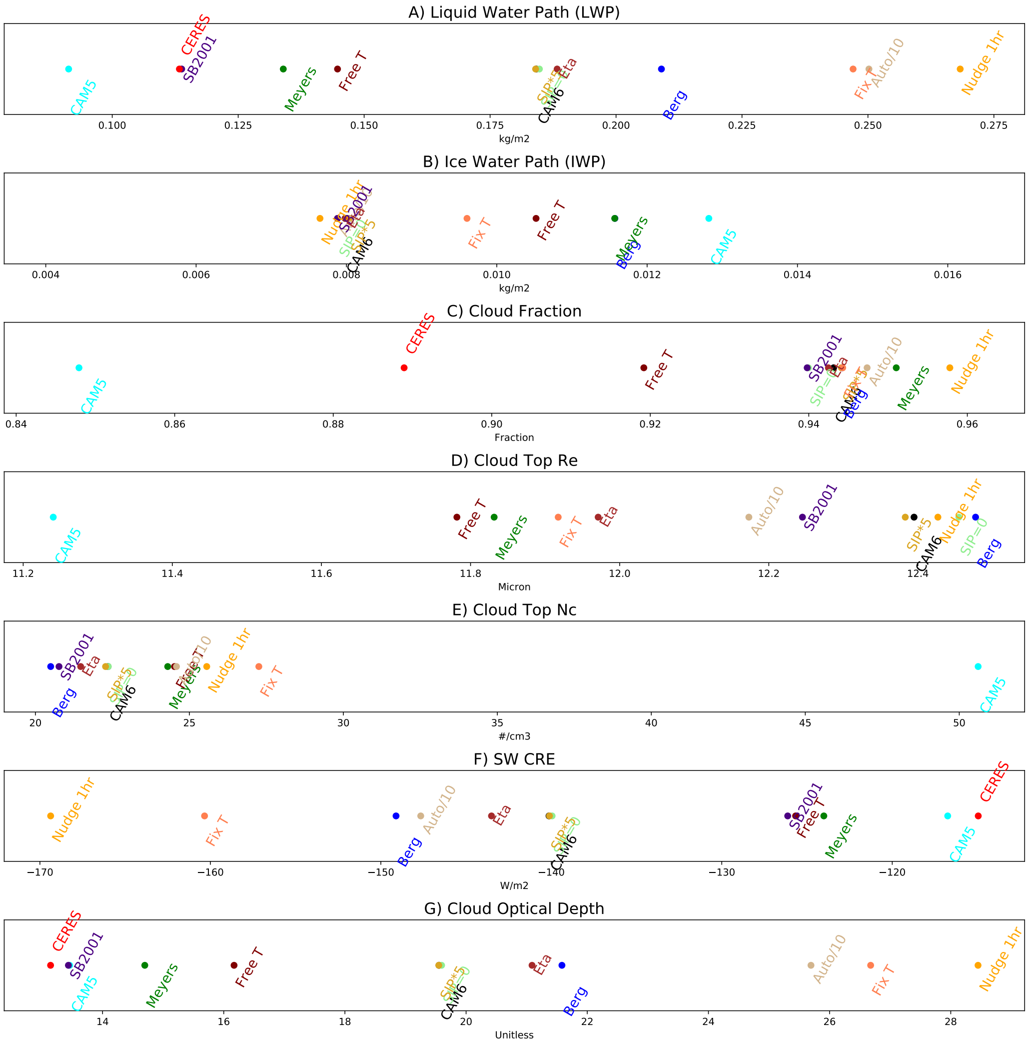

Figure 11. Jan-Feb 2018 2 month Mean over 65-45 °S and 135-160 °E of (A) Liquid Water Path (TGCLDLWP), (B) Ice Water Path (TGCLDIWP), (C) Total Cloud Cover (CLDTOT), (D) Cloud Top Effective Radius (ACTREL), (E) Cloud Top Drop Number Concentration (ACTNL), (F) Top of Atmosphere Short Wave Cloud Radiative Effect (SW CRE), (G) Total cloud optical depth. Sensitivity tests from CAM as described in Table 1 in blue, and CERES observations in Red where available.

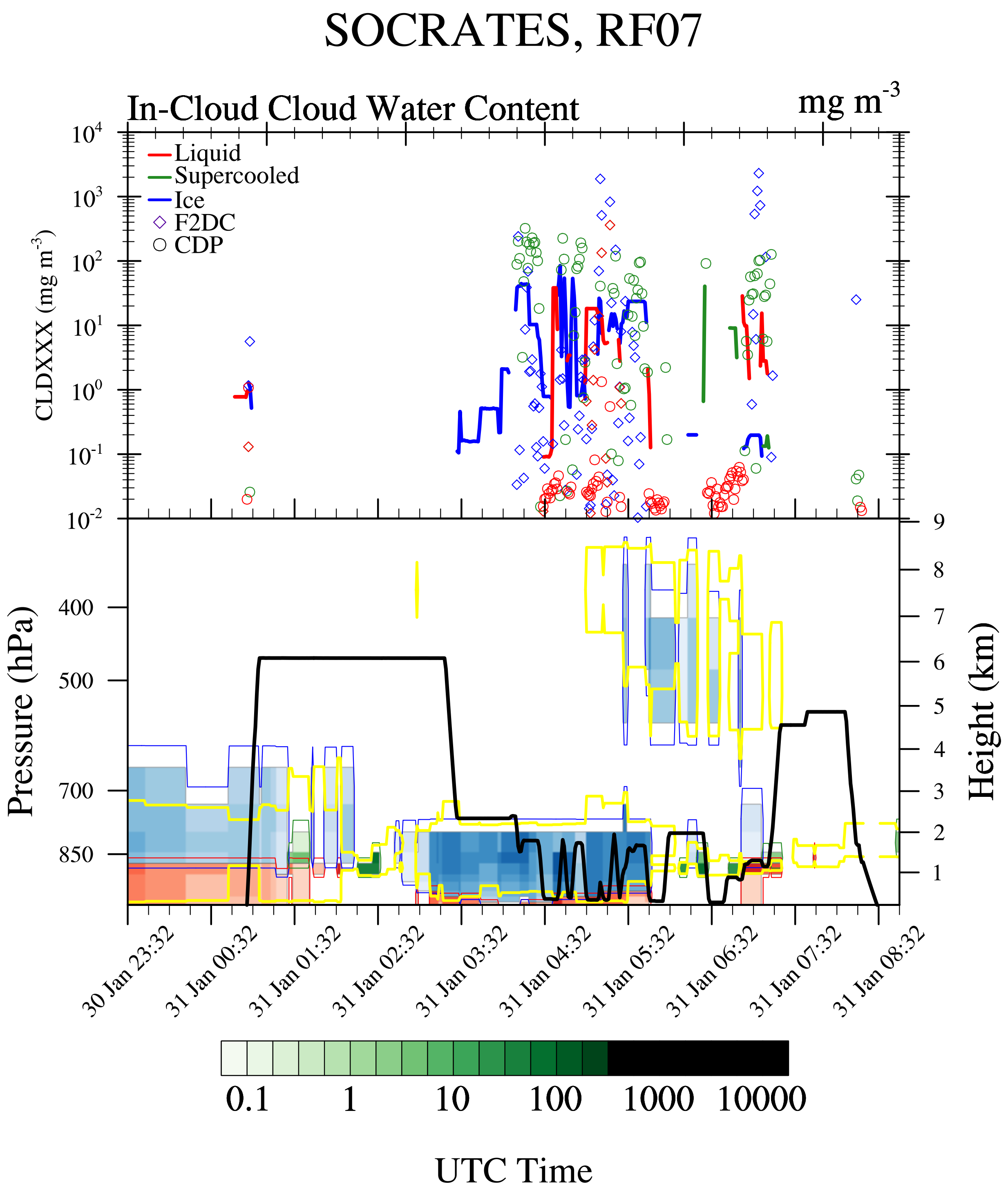

Figure 12. As for Figure 9 but for a simulation using 'CAM5' physical parameterizations.

3.3 Global Implications

Finally we look at the longer term and global implications of these results. The different model formulations do not just have different results in the S. Ocean, but their climate is different globally. We have tested *CAM5*, *CAM6 Meyers* and *SB2001* formulations. These simulations are detailed in Gettelman et al. (2019). Simulations are similar to the nudged runs (same code basis, same resolution) but run with climatological Sea Surface Temperatures and no nudging. Simulations are 10 years long.

Figure 13 illustrates four different configurations of 10 year long free running CAM simulations compared to a long term annual climatology from 15 years of CERES EBAF 4.1 data. Here some of the results of Figure 11 can be put into context. In the S. Ocean, over all longitudes, SOCRATES region between 65-45 °S, *CAM5* has too weak SWCRE and LWCRE relative to CERES. The SWCRE is too strong in *CAM6*, while the *SB2001* formulation is much closer to CERES observations. This is consistent with Figure 11 in the smaller SOCRATES region. However, the LWCRE has less bias in *CAM6* and *SB2001* and the tropics are significantly better. The SOCRATES region seasonal (DJF) SW Root Mean Square Error (RMSE) between the CAM simulations and CERES EBAF4.1 is larger for *CAM6* (24 Wm^{-2}) than *CAM5* (9.7 Wm^{-2}) but the Global Annual RMSE is smaller for *CAM6* (9.1 Wm^{-2}) than *CAM5* (12.4 Wm^{-2}) while CAM6 with Meyers et al. (1992) ice nucleation (*Meyers*) is intermediate between them. The use of Seifert & Beheng (2001) autoconversion (*SB2001*) yields lower RMSE versus CERES than CAM6 for the SOCRATES region seasonal DJF RMSE (16 Wm^{-2}), and the lowest global RMSE (8.2 Wm^{-2}).

The difference in mean state yields a different climate response. As noted by Gettelman et al. (2019), CAM5 and CAM6 have different climate sensitivity (the surface temperature response to an imposed forcing) which was found to be a result of different cloud feedbacks (the radiative response of clouds to surface warming). Gettelman et al. (2019) found that this difference was partially due to high latitude cloud processes and the different distribution of supercooled liquid water. As noted by Tan et al. (2016) and others, without supercooled liquid (CAM5) there is a negative cloud phase feedback when ice clouds become liquid in a warmer world. But if these clouds are supercooled liquid (CAM6), this negative feedback is not present.

4 Discussion

CAM6 nudged simulations do a remarkably good job in capturing SOCRATES observations of clouds and cloud microphysics. The nudging technique reproduces cloud regimes in similar locations to the aircraft, particularly with respect to supercooled liquid clouds. There are some biases in the structure of the inversion at the top of boundary layer in the simulations, which can be partially mitigated by fixing temperatures to the input data. Setting nudging timescales and parameters (whether to nudge temperature or not) will affect the cloud simulation, and while temperatures may move closer to observations (Figure 7), cloud simulation (cloud fraction, cloud phase, water content, and radiative effects) may change significantly and be further from CERES observations (Figure 11).

Given these caveats about the method, the resulting cloud properties agree quite well with SOCRATES observations on individual flights, particularly given the scale separation between model and observations. Supercooled liquid clouds are produced extensively in cold sectors of cyclones in the S. Ocean targeted by SOCRATES. Supercooled liquid is better than in previous versions (CAM5) and this is largely due to the new mixed phase ice nucleation which is now dependent on available ice nuclei rather than an empirical function of temperature.

Cloud hydrometeor size distributions are also broadly reproduced across both ice and liquid from small cloud drops to large rain and snow particles. The model has some

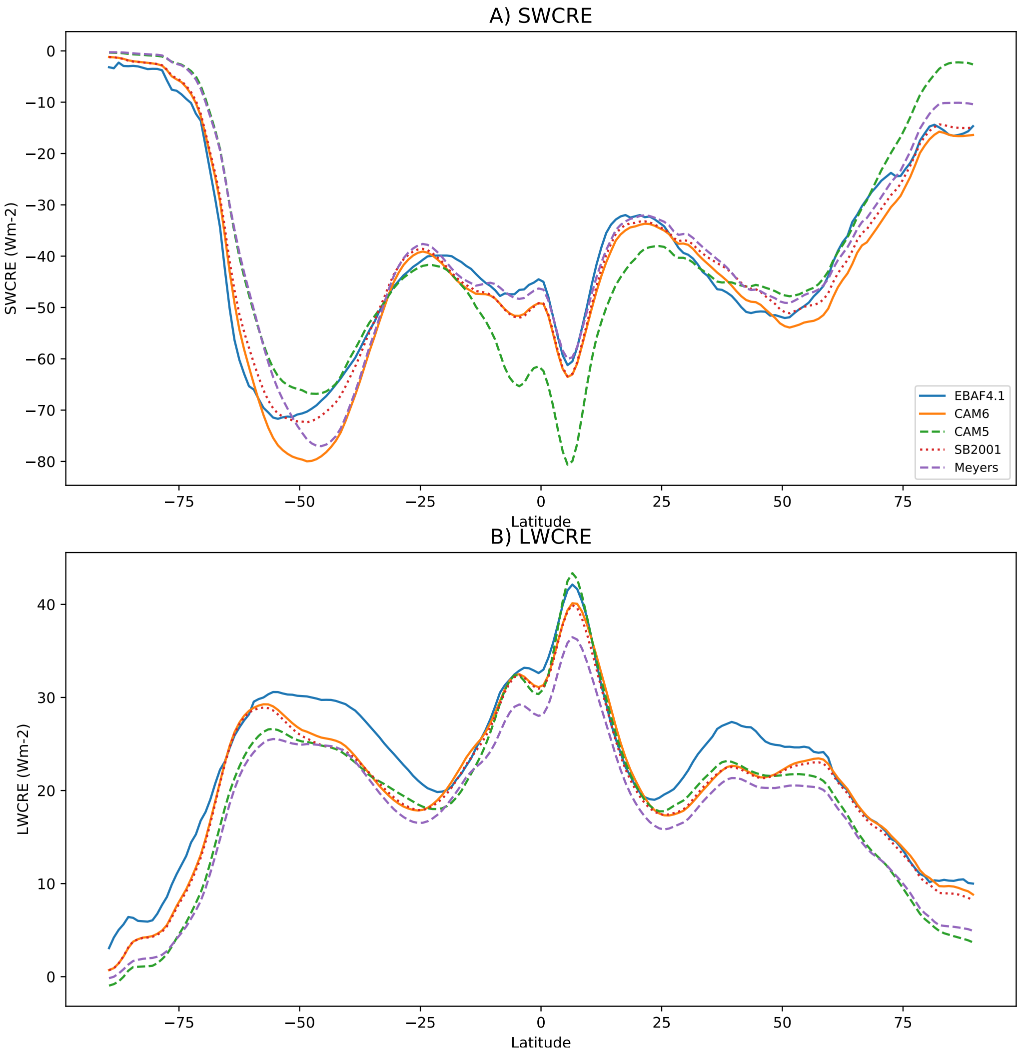

Figure 13. Zonal annual mean climatology of (A) SW and (B) LW Cloud radiative effects from CAM simulations and CERES observations (EBAF4.1).

systematic deficiencies however. For warm clouds, there may be too much mass of rain, particularly around 100 micron diameter. For cold clouds, snow is well reproduced, but supercooled droplet size distributions tend to have too few numbers and an insufficient peak in the size distribution at 10-20 microns. Modifcation of the dispersion of the size distribution does improve these results slightly, but does not increase overall drop numbers. Overall number is increased by reducing autoconversion.

Achieving radiative closure for cloud microphysics and radiation is difficult, even with observations. The *CAM5* simulated LWP over the entire region and period is 50% lower than *CAM6* (Figure 11A) and the IWP is 50% higher (Figure 11B). This likely leads to the lower cloud fraction (Figure 11C) and ultimately weaker SW CRE (Figure 11F) and lower optical depth (Figure 11G) simulated by *CAM5* compared to *CAM6*. Small (Figure 11D) and numerous (Figure 11E drops compensate for low LWP. Meanwhile, in situ observations from SOCRATES suggest that the dominant cloud phase simulated in *CAM5* (ice) is far different from observed (supercooled liquid) and the cloud location (boundary layer top) also differs in *CAM5*. CERES also retrieves more ice than liquid, which does not match SOCRATES in-situ observations. These comparisons call into question cloud products from the broader CERES observations in Figure 11. However, the *SB2001* experiment looks much closer to the CERES observations for LWP and SW CRE with less water, while maintaining significant supercooled liquid water (similar to *CAM6*), demonstrating that multiple physical processes (ice nucleation, autoconversion) likely play an important role in how S. Ocean clouds are represented in CAM6.

The size distribution biases may contribute to the inability to reproduce the zonal mean structure of overall climatological cloud radiative effect, and having too few cloud drops may imply a larger mean size. However, the experiments with adjusted autoconversion indicate that lower water path (found in SB2001) can also improve the comparisons with observations. The mass seems to be the first order effect, with size distributions a second order effect. However, with larger drops it may be possible to maintain a larger liquid water path. Note that the CERES LWP product assumes a 10 micron size, so comparisons with in-situ observations are perhaps more relevant.

This analysis with observations provides a process (and observationally constrained) pathway to improve simulations further. Better constraints on condensate mass from the observations are still being developed for SOCRATES, and these will be valuable in adding an additional constraint on the the simulations and resulting radiative properties. Because cloud feedbacks and climate sensitivity are dependent on the microphysics (phase, water content) of S. Ocean clouds, this is critical for constraining climate projections. SOCRATES observations confirm that SO clouds are mostly supercooled liquid, similar to CAM6.

5 Conclusions

Nudged simulations with a global climate model (CAM6) even at coarse horizontal and vertical resolution are able to capture many of the important features of specific cloud systems observed by SOCRATES. Successful simulations have some biases in the boundary layer structure related to vertical resolution and to nudging itself, and some care must be taken in understanding the purpose of nudging as changing the temperature structure changes the overall cloud simulation. The fact that improving the temperatures relative to analysis temperatures may degrade the overall cloud simulation indicates problems fitting one model (CAM) to another model (MERRA2) state and/or compensating biases in CAM.

Comparisons between model and observations for flights into supercooled liquid clouds during SOCRATES show that improvements to the ice nucleation scheme in CAM6 result in significant improvements in the representation of supercooled liquid water. CAM is not sensitive to Secondary Ice Production in the SO region, but is sensitive to ice nucleation, and changes in warm rain formation (autoconversion).

One of the most unique features of this study is the ability to compare detailed cloud microphysics (phase and size distributions of different hydrometeors) across scales between large scale models and in-situ observations. This works particularly well in the relatively uniform cloud regimes observed during SOCRATES RF07 and other SOCRATES flights.

However, biases remain, and cloud closure between microphysics and radiation is difficult. While the overall microphysics and phase of clouds in CAM6 looks quite good for SOCRATES clouds, when a broader climatological picture is explored over the SOCRATES region, there are significant biases in radiative fluxes. The details of the cloud physics might be creating biases such that the right radiative response is occurring for the wrong reasons in either the model or satellite retreivals. The radiative response can be improved with less water path through the use of a revised autoconversion scheme (*SB2001*), but still does not match droplet numbers seen in the aircraft observations. It is likely that the CERES retrievals of microphysics (LWP and IWP) from radiative fluxes have significant biases due to fixed specification of particle size. This makes comparisons with satellite retrievals from the top of the atmosphere difficult to compare, not least because of uncertainty in the satellite retrievals themselves, which is a useful subject for further study against SOCRATES data.

Because model formulations with different cloud microphysics (i.e., CAM6 and CAM5) have different high latitude cloud feedbacks, it is critical to understand and constrain the phase partitioning and cloud microphysics of S. Ocean clouds. In this case, CAM6 with more supercooled liquid and more positive cloud feedbacks (and higher climate sensitivity) looks more physically plausible in the S. Ocean due to better cloud phase simulation.

These results should be tested against different scales of cloud models for the SOCRATES regime, and against different global simulations. In addition, better constraints on in-situ observed condensate mass would be useful for better constraining the observations. There are still large uncertainties in the retrieval of condensate mass from the in-situ cloud probes and is thus the focus of a separate manuscript.

In particular, advanced 2-moment cloud physics schemes such as Gettelman & Morrison (2015) provide more detail about potential causes for discrepancies against observations, and a multi-scale observational approach from in-situ microphysics to satellite data provides unprecedented detail that has and can continue to help guide model improvements in this critical region for climate projections.

Acknowledgments

The National Center for Atmospheric Research is sponsored by the U.S. National Science Foundation. Work under this project was performed with a generous grant from the Climate and Global Dynamics Program of the US NSF (NSF-UWSC9960) to NCAR and the University of Washington. We thank all the hard work from the EOL and Science Teams for the SOCRATES project for collecting the data used in this project. All observation data is available from the NCAR Earth Observation Lab (EOL) Field Catalog (http://catalog.eol.ucar.edu/socrates). Model simulations. Model simulations are available on the Earth System Grid (https://www.earthsystemgrid.org/) using the manuscript DOI.

References

Bodas-Salcedo, A., Williams, K., Field, P., & Lock, A. (2012). The surface down-

welling solar radiation surplus over the Southern Ocean in the Met Office model: The role of midlatitude cyclone clouds. *J. Climate*, *25*(21), 7467–7486.
Bodas-Salcedo, A., Mulcahy, J. P., Andrews, T., Williams, K. D., Ringer, M. A., Field, P. R., & Elsaesser, G. S. (2019). Strong Dependence of Atmospheric Feedbacks on Mixed-Phase Microphysics and Aerosol-Cloud Interactions in HadGEM3. *Journal of Advances in Modeling Earth Systems*, *11*(6), 1735–1758. doi: 10.1029/2019MS001688
Bogenschutz, P. A., Gettelman, A., Morrison, H., Larson, V. E., Craig, C., & Schanen, D. P. (2013). Higher-order turbulence closure and its impact on Climate Simulation in the Community Atmosphere Model. *Journal of Climate*, *26*(23), 9655–9676. doi: 10.1175/JCLI-D-13-00075.1
Bretherton, C. S., & Park, S. (2009). A new moist turbulence parameterization in the Community Atmosphere Model. *joc*, *22*, 3422–3448.
Cotton, W. R., Tripoli, G. J., Rauber, R. M., & Mulvihill, E. A. (1986). Numerical simulation of the effects of varying ice crystal nucleation rates and aggregation processes on orographic snowfall. *J. Appl. Meteor.*, *25*, 1658–1680.
Danabasoglu, G., Lamarque, J.-F., Bacmeister, J., Bailey, D. A., DuVivier, A. K., Edwards, J., … Strand, W. G. (2020). The Community Earth System Model Version 2 (CESM2). *Journal of Advances in Modeling Earth Systems*, *12*(2), e2019MS001916. doi: 10.1029/2019MS001916
EOL. (2018). *SOCRATES 2018 Project Manager Report)* (Tech. Rep.). NCAR - Earth Observing Laboratory.
Gettelman, A. (2015, November). Putting the clouds back in aerosol–cloud interactions. *Atmos. Chem. Phys.*, *15*(21), 12397–12411. doi: 10.5194/acp-15-12397-2015
Gettelman, A., Hannay, C., Bacmeister, J. T., Neale, R. B., Pendergrass, A. G., Danabasoglu, G., … Mills, M. J. (2019). High Climate Sensitivity in the Community Earth System Model Version 2 (CESM2). *Geophysical Research Letters*, *0*(0). doi: 10.1029/2019GL083978
Gettelman, A., Liu, X., Ghan, S. J., Morrison, H., Park, S., Conley, A. J., … Li, J.-L. F. (2010). Global Simulations of Ice nucleation and Ice Supersaturation with an Improved Cloud Scheme in the Community Atmosphere Model. *J. Geophys. Res.*, *115*(D18216). doi: 10.1029/2009JD013797
Gettelman, A., & Morrison, H. (2015). Advanced Two-Moment Bulk Microphysics for Global Models. Part I: Off-Line Tests and Comparison with Other Schemes. *J. Climate*, *28*(3), 1268–1287. doi: 10.1175/JCLI-D-14-00102.1
Gettelman, A., Morrison, H., Santos, S., Bogenschutz, P., & Caldwell, P. M. (2015). Advanced Two-Moment Bulk Microphysics for Global Models. Part II: Global Model Solutions and Aerosol–Cloud Interactions. *J. Climate*, *28*(3), 1288–1307. doi: 10.1175/JCLI-D-14-00103.1
Golaz, J.-C., Larson, V. E., & Cotton, W. R. (2002). A PDF-Based Model for Boundary Layer Clouds. Part II: Model Results. *J. Atmos. Sci.*, *59*, 3552–3571.
Hoose, C., Kristjánsson, J. E., Chen, J.-P., & Hazra, A. (2010, March). A Classical-Theory-Based Parameterization of Heterogeneous Ice Nucleation by Mineral Dust, Soot, and Biological Particles in a Global Climate Model. *J. Atmos. Sci.*, *67*(8), 2483–2503. doi: 10.1175/2010JAS3425.1
Iacono, M. J., Mlawer, E. J., Clough, S. A., & Morcrette, J.-J. (2000). Impact of an improved longwave radiation model, RRTM, on the energy budget and thermodynamic properties of the NCAR community climate model, CCM3. *jgr*, *105*(D11), 14,873–14,890.
Khairoutdinov, M. F., & Kogan, Y. (2000). A new cloud physics parameterization in a large-eddy simulation model of marine stratocumulus. *Monthly Weather Review*, *128*, 229–243.
King, W. D., Parkin, D. A., & Handsworth, R. J. (1978, December). A Hot-Wire

Liquid Water Device Having Fully Calculable Response Characteristics. *J. Appl. Meteor.*, *17*(12), 1809–1813. doi: 10.1175/1520-0450(1978)017⟨1809:AHWLWD⟩2.0.CO;2

Lance, S., Brock, C. A., Rogers, D., & Gordon, J. A. (2010, December). Water droplet calibration of the Cloud Droplet Probe (CDP) and in-flight performance in liquid, ice and mixed-phase clouds during ARCPAC. *Atmospheric Measurement Techniques*, *3*(6), 1683–1706. doi: https://doi.org/10.5194/amt-3-1683-2010

Larson, V. E., Golaz, J.-C., & Cotton, W. R. (2002, December). Small-Scale and Mesoscale Variability in Cloudy Boundary Layers: Joint Probability Density Functions. *J. Atmos. Sci.*, *59*(24), 3519–3539. doi: 10.1175/1520-0469(2002)059⟨3519:SSAMVI⟩2.0.CO;2

Liu, X., & Penner, J. E. (2005). Ice Nucleation Parameterization for Global Models. *Meteor. Z.*, *14*(499-514).

Loeb, N. G., Doelling, D. R., Wang, H., Su, W., Nguyen, C., Corbett, J. G., … Kato, S. (2018). Clouds and the Earth's Radiant Energy System (CERES) Energy Balanced and Filled (EBAF) Top-of-Atmosphere (TOA) Edition-4.0 Data Product. *J. Climate*, *31*(2), 895–918. doi: 10.1175/JCLI-D-17-0208.1

Lohmann, U., & Neubauer, D. (2018, June). The importance of mixed-phase and ice clouds for climate sensitivity in the global aerosol–climate model ECHAM6-HAM2. *Atmospheric Chemistry and Physics*, *18*(12), 8807–8828. doi: https://doi.org/10.5194/acp-18-8807-2018

Mace, G. G., & Protat, A. (2018, April). Clouds over the Southern Ocean as Observed from the R/V Investigator during CAPRICORN. Part I: Cloud Occurrence and Phase Partitioning. *J. Appl. Meteor. Climatol.*, *57*(8), 1783–1803. doi: 10.1175/JAMC-D-17-0194.1

Martin, G. M., Johnson, D. W., & Spice, A. (1994). The measurement and parameterization of effective radius of droplets in warm stratocumulus clouds. *J. Atmos. Sci.*, *51*, 1823–1842.

McCluskey, C. S., Hill, T. C. J., Humphries, R. S., Rauker, A. M., Moreau, S., Strutton, P. G., … DeMott, P. J. (2018). Observations of Ice Nucleating Particles Over Southern Ocean Waters. *Geophysical Research Letters*, *45*(21), 11,989–11,997. doi: 10.1029/2018GL079981

Meyers, M. P., DeMott, P. J., & Cotton, W. R. (1992). New Primary Ice-Nucleation Parameterizations in an Explicit Cloud Model. *J. Applied Met.*, *31*, 708–721.

Molod, A., Takacs, L., Suarez, M., & Bacmeister, J. (2015, May). Development of the GEOS-5 atmospheric general circulation model: Evolution from MERRA to MERRA2. *Geosci. Model Dev.*, *8*(5), 1339–1356. doi: 10.5194/gmd-8-1339-2015

Morrison, H., & Gettelman, A. (2008). A new two-moment bulk stratiform cloud microphysics scheme in the NCAR Community Atmosphere Model (CAM3), Part I: Description and Numerical Tests. *J. Climate*, *21*(15), 3642–3659.

Neale, R. B., Chen, C. C., Gettelman, A., Lauritzen, P. H., Park, S., Williamson, D. L., … Taylor, M. A. (2010). *Description of the NCAR Community Atmosphere Model (CAM5.0)* (Tech. Rep. Nos. NCAR/TN-486+STR). Boulder, CO, USA: National Center for Atmospheric Research.

Neale, R. B., Richter, J. H., & Jochum, M. (2008). The Impact of Convection on ENSO: From a Delayed Oscillator to a Series of Events. *J. Climate*, *21*, 5904-+. doi: 10.1175/2008JCLI2244.1

O'Shea, S. J., Choularton, T. W., Flynn, M., Bower, K. N., Gallagher, M., Crosier, J., … Lachlan-Cope, T. (2017, November). In situ measurements of cloud microphysics and aerosol over coastal Antarctica during the MAC campaign. *Atmospheric Chemistry and Physics*, *17*(21), 13049–13070. doi: https://doi.org/10.5194/acp-17-13049-2017

Park, S., & Bretherton, C. S. (2009). The University of Washington shallow convection and moist turbulence schemes and their impact on climate simulations with the Community Atmosphere Model. *J. Climate*, *22*, 3449–3469.

Rotstayn, L. D., & Liu, Y. (2003, November). Sensitivity of the First Indirect Aerosol Effect to an Increase of Cloud Droplet Spectral Dispersion with Droplet Number Concentration. *J. Climate*, *16*(21), 3476–3481. doi: 10.1175/1520-0442(2003)016⟨3476:SOTFIA⟩2.0.CO;2

Seifert, A., & Beheng, K. D. (2001). A double-moment parameterization for simulating autoconversion, accretion and selfcollection. *Atmos. Res.*, *59-60*, 265–281.

Shi, X., Liu, X., & Zhang, K. (2015, February). Effects of pre-existing ice crystals on cirrus clouds and comparison between different ice nucleation parameterizations with the Community Atmosphere Model (CAM5). *Atmospheric Chemistry and Physics*, *15*(3), 1503–1520. doi: 10.5194/acp-15-1503-2015

Tan, I., Storelvmo, T., & Zelinka, M. D. (2016, April). Observational constraints on mixed-phase clouds imply higher climate sensitivity. *Science*, *352*(6282), 224–227. doi: 10.1126/science.aad5300

Trenberth, K. E., & Fasullo, J. T. (2010). Simulation of Present-Day and Twenty-First-Century Energy Budgets of the Southern Oceans. *J. Climate*, *23*, 440–454. doi: 10.1175/2009JCLI3152.1

Tsushima, Y., Emori, S., Ogura, T., Kimoto, M., Webb, M. J., Williams, K. D., ... Andronova, N. (2006). Importance of the mixed-phase cloud distribution in the control climate for assessing the response of clouds to carbon dioxide increase: A multi-model study. *Clim. Dyn.*, *27*, 113–126. doi: 10.1007/s00382-006-0127-7

Vergara-Temprado, J., Miltenberger, A. K., Furtado, K., Grosvenor, D. P., Shipway, B. J., Hill, A. A., ... Carslaw, K. S. (2018, February). Strong control of Southern Ocean cloud reflectivity by ice-nucleating particles. *PNAS*, 201721627. doi: 10.1073/pnas.1721627115

Wang, Y., Liu, X., Hoose, C., & Wang, B. (2014, October). Different contact angle distributions for heterogeneous ice nucleation in the Community Atmospheric Model version 5. *Atmos. Chem. Phys.*, *14*(19), 10411–10430. doi: 10.5194/acp-14-10411-2014

Wielicki, B. A., Barkstrom, B. R., Harrison, E. F., III, R. B. L., Smith, G. L., & Cooper, J. E. (1996). Clouds and the Earth's Radiant Energy System (CERES): An Earth Observing System Experiment. *bams*, *77*(5), 853–868.

Young, K. (2018). *NCAR/EOL Quality Controlled Dropsonde Data. Version 1.0* (Tech. Rep.). NCAR - Earth Observing Laboratory.

Young, K., & Vömel, H. (2018). *SOCRATES 2018 NCAR/EOL Dropsonde Data Quality Report* (Tech. Rep.). NCAR - Earth Observing Laboratory.

Zhang, G. J., & McFarlane, N. A. (1995). Sensitivity of climate simulations to the parameterization of cumulus convection in the Canadian Climate Center general circulation model. *Atmos. Ocean*, *33*, 407–446.